

# IEEE GEOSCIENCE AND REMOTE SENSING LETTERS

A PUBLICATION OF THE IEEE GEOSCIENCE AND REMOTE SENSING SOCIETY



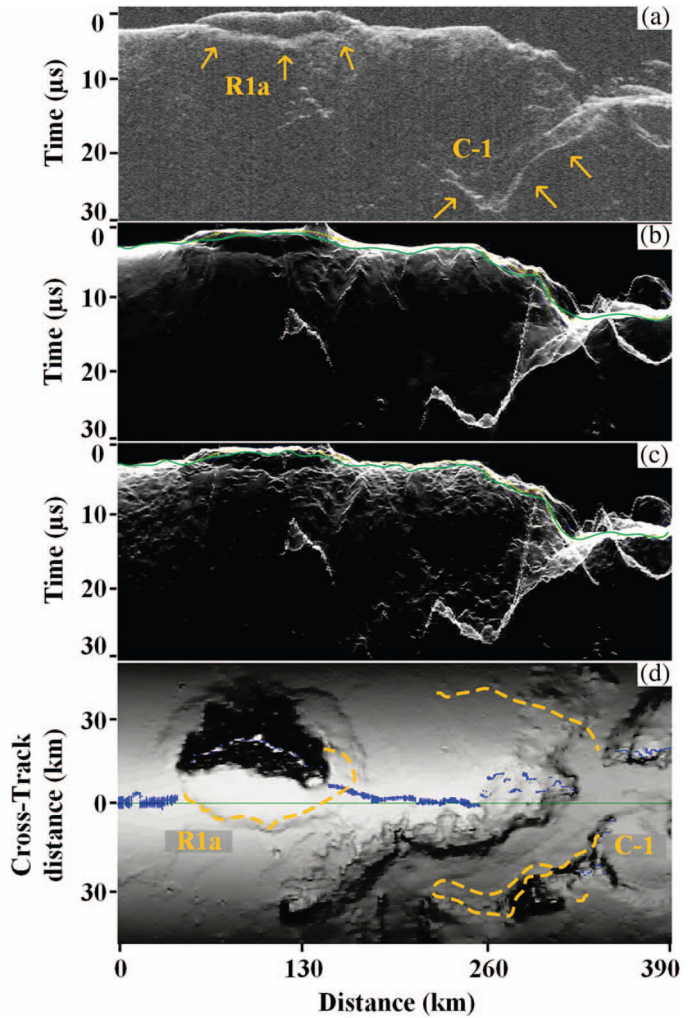
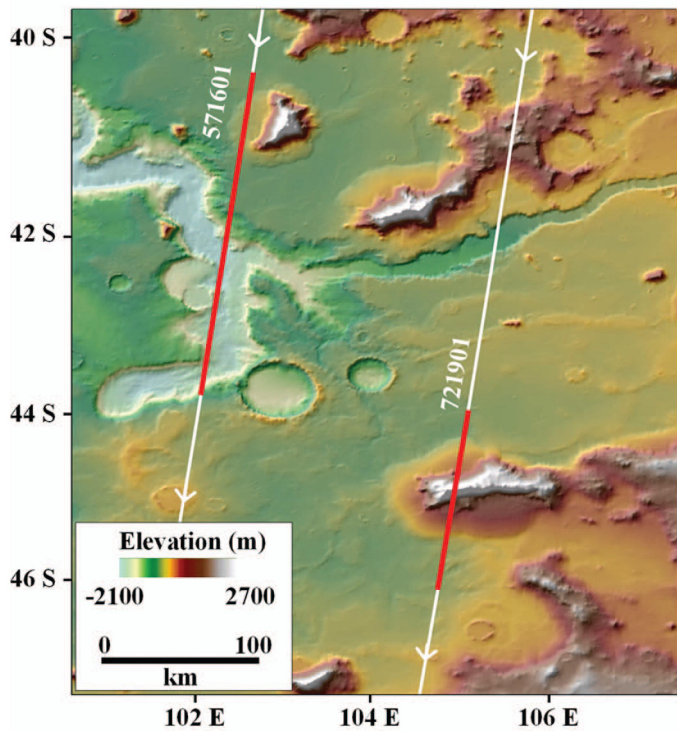
SEPTEMBER 2016

VOLUME 13

NUMBER 9

IGRSBY

(ISSN 1545-598X)



SHARAD orbital radar sounding data from Mars with predicted surface clutter and echo locations to aid in interpretation.

IEEE

# GEOSCIENCE AND REMOTE SENSING LETTERS

A PUBLICATION OF THE IEEE GEOSCIENCE AND REMOTE SENSING SOCIETY



SEPTEMBER 2016

VOLUME 13

NUMBER 9

IGRSBY

(ISSN 1545-598X)

---

## PAPERS

### Atmosphere

- Analyzing the Hydroclimatic Teleconnections of Summer Monsoon Rainfall in Kerala, India, Using Multivariate Empirical Mode Decomposition and Time-Dependent Intrinsic Correlation . . . . . A. Sankaran and M. Janga Reddy 1221

### Oceans and Water

- Effect of the Local Backscattering Pattern of the Sea Surface to the Reflected Signal of a Precision Airborne Radar Altimeter at Low Altitude . . . . . M.-H. Ka, A. I. Baskakov, and A. Artemenko 1246  
Analysis of Dual-Frequency Ocean Backscatter Measurements at Ku- and Ka-Bands Using Near-Nadir Incidence GPM Radar Data . . . . . F. Nouguier, A. Mouche, N. Rascle, B. Chapron, and D. Vandemark 1310  
Sensor Placement for Underwater Source Localization With Fixed Distances . . . . . X. Fang, W. Yan, and W. Chen 1379

### Vegetation and Land Surface

- An Algorithm for Retrieving Soil Moisture Using L-Band H-Polarized Multiangular Brightness Temperature Data . . . . . Q. Cui, X. Dong, J. Shi, T. Zhao, and C. Xiong 1295

### Surface and Subsurface Properties

- Surface Clutter and Echo Location Analysis for the Interpretation of SHARAD Data From Mars . . . . . P. Choudhary, J. W. Holt, and S. D. Kempf 1285  
Radar Backscattering Coefficient Over Bare Soils at Ka-Band Close to Nadir Angle . . . . . C. Fatras, P. Borderies, N. Baghdadi, M. Zribi, M. El Hajj, F. Frappart, and E. Mougin 1290  
Understanding Well Log Peak Shifts in Thin Beds . . . . . F. Wu, Z. Wen, X. Liang, W. Yu, J. Ma, and L. Sima 1345  
Interpolating Big Gaps Using Inversion With Slope Constraint . . . . . S. Zu, H. Zhou, Y. Chen, X. Pan, S. Gan, and D. Zhang 1369  
An Efficient POCS Interpolation Method in the Frequency-Space Domain . . . . . B. Wang 1384

### Image Processing, Analysis, and Classification

- Edge-Based Registration-Noise Estimation in VHR Multitemporal and Multisensor Images . . . . . Y. Han, F. Bovolo, and L. Bruzzone 1231  
Remote Sensing Optical Image Registration Using Modified Uniform Robust SIFT . . . . . S. Paul and U. C. Pati 1300  
Reliable Subpixel Ground Control Point Estimation Algorithm Using Vector Roads . . . . . J. Zaleletelj 1325  
Reduction of Spectral Unmixing Uncertainty Using Minimum-Class-Variance Support Vector Machines . . . . . X. Li, X. Jia, L. Wang, and K. Zhao 1335  
Metaheuristics for Supervised Parameter Tuning of Multiresolution Segmentation . . . . . V. A. Ayma Quirita, P. Achancaray Diaz, R. Q. Feitosa, P. N. Happ, G. A. O. P. Costa, T. Klinger, and C. Heipke 1364  
A Morphological Building Detection Framework for High-Resolution Optical Imagery Over Urban Areas . . . . . Q. Zhang, X. Huang, and G. Zhang 1388
- 

(Contents Continued on Page 1210)

---

<b>Hyperspectral Data Processing</b>	
Tangent Distance-Based Collaborative Representation for Hyperspectral Image Classification . . . . .	1236
Hyperspectral Image Super-Resolution by Spectral Mixture Analysis and Spatial-Spectral Group Sparsity . . . . .	1250
Fast SVD With Random Hadamard Projection for Hyperspectral Dimensionality Reduction . . . . .	1275
<b>Radar Systems</b>	
Comparative Analysis of Two Approaches for Multipath Ghost Suppression in Radar Imaging . . . . .	1226
A Modified Adaptive Sidelobe Reduction Method for Through-the-Wall Radar Imaging . . . . .	1255
A Weighted Backprojection Algorithm for Azimuth Multichannel SAR Imaging . . . . .	1265
First-Order Multipath Ghosts' Characteristics and Suppression in MIMO Through-Wall Imaging . . . . .	1315
Micro-Doppler Analysis of Rigid-Body Targets via Block-Sparse Forward–Backward Time-Varying Autoregressive Model . . . . .	1349
<b>Microwave Radiometry</b>	
Interelement Phase Calibration for the Geostationary Interferometric Microwave Sounder (GIMS) . . . . .	1216
Global Land Surface Emissivity Estimation From AMSR2 Observations . . . . .	1270
Implementation of Advanced Carrier Tracking Algorithm Using Adaptive-Extended Kalman Filter for GNSS Receivers . . . . .	1280
Noise Limitations on the Recovery of Average Values of Velocity Profiles in Pipelines by Simple Imaging Systems . . . . .	1340
<b>Synthetic Aperture Radar</b>	
Forward Velocity Extraction From UAV Raw SAR Data Based on Adaptive Notch Filtering . . . . .	1211
Multiple Local Autofocus Back-Projection Algorithm for Space-Variant Phase-Error Correction in Synthetic Aperture Radar . . . . .	1241
Clutter-Cancellation-Based Channel Phase Bias Estimation Algorithm for Spaceborne Multichannel High-Resolution and Wide-Swath SAR . . . . .	1260
Classification of Birds and UAVs Based on Radar Polarimetry . . . . .	1305
Inland Water Height Estimation Without Ground Control Points for Near-Nadir InSAR Data . . . . .	1354
Stacked Sparse Autoencoder in PolSAR Data Classification Using Local Spatial Information . . . . .	1359
<b>Lidar Systems</b>	
Individual Tree Delineation in Windbreaks Using Airborne-Laser-Scanning Data and Unmanned Aerial Vehicle Stereo Images . . . . .	1330
<b>APSAR 2015</b>	
Moving Target Detection via Efficient ATI-GoDec Approach for Multichannel SAR System . . . . .	1320
A Parameter Optimization Model for Geosynchronous SAR Sensor in Aspects of Signal Bandwidth and Integration Time . . . . .	1374

---

About the Cover: Shallow Radar (SHARAD) onboard the Mars Reconnaissance Orbiter (MRO) has been mapping the Martian subsurface since November 2006. Some of SHARAD's primary scientific objectives are to identify the presence of water ice deposits and to study the internal structure of polar ice deposits. Radar returns from cross-track surface features have longer time delay than returns from nadir, and can be confused as returns from below the surface. Simulating such returns ("surface clutter") is crucial for analyzing SHARAD data with confidence. Furthermore, even small cross-track slopes can significantly move the primary return from the nadir location, impacting the perceived source of subsurface echoes. This clutter simulator has been used to identify water-ice in the southern midlatitudes of Mars, identify proposed landing sites, and generate 3-D maps of subsurface interfaces. For more information please see "Surface Clutter and Echo Location Analysis for the Interpretation of SHARAD Data From Mars" by Choudhary *et al.*, which begins on page 1285.